CERN/SPSC 2001/002 – SPSC/P320
December 14, 2000

SW:200103

Proposal to the SPSC

Measurement of the ELastic Anti Proton Proton Cross Section at AD

The ELAPP Collaboration

M. Agnello[a], M. Astrua[b], E. Botta[b], T. Bressani[b 1], L. Busso[c], D. Calvo[b], A. Feliciello[b], A. Filippi[b], F. Iazzi[a], S. Marcello[b], O. Morra[d], V. Mussino[a], G. Rizzi[a]

[a]*Politecnico di Torino and INFN, Sezione di Torino, Torino, Italy*

[b]*Dipartimento di Fisica Sperimentale, Università di Torino, and INFN, Sezione di Torino, Torino, Italy*

[c]*Dipartimento di Fisica Generale "A. Avogadro", Università di Torino and INFN, Sezione di Torino, Torino, Italy*

[d]*CNR, Istituto di Cosmogeofisica, and INFN, Sezione di Torino, Torino, Italy*

[1]Spokeperson, e-mail address: bressani@to.infn.it

Introduction

We propose the measurement of the elastic $\bar{p}p$ cross section in the momentum region (50÷140) MeV/c (lab.) at the AD machine at CERN. The lack of experimental data in this range together with quite anomalous behaviours in the $\bar{N}N$ data existing in literature are the main reasons for this proposal; these arguments will be discussed in the Chapter 1.

At present, AD is the only machine in the world which can supply $\bar{p}$'s of such low energies, although it has been designed for different goals: the problems arising from its specific features (high intensity, short duration bursts) will be discussed in Chapter 2, where suitable solutions are proposed. In Chapter 3 the technique of the measurements is described and in Chapter 4 a look at a possible future extension of the physics program is given.

Contents

Chapter 1

Physics motivations

A very recent measurement by OBELIX [1] of the $\bar{n}p$ total cross section $\sigma_{tot}(\bar{n}p)$ from 50 to 400 MeV/c (lab.) showed a quite interesting and unexpected behaviour below 100 MeV/c. Fig. 1.1 shows the measured $\sigma_{tot}(\bar{n}p)$, together with the only

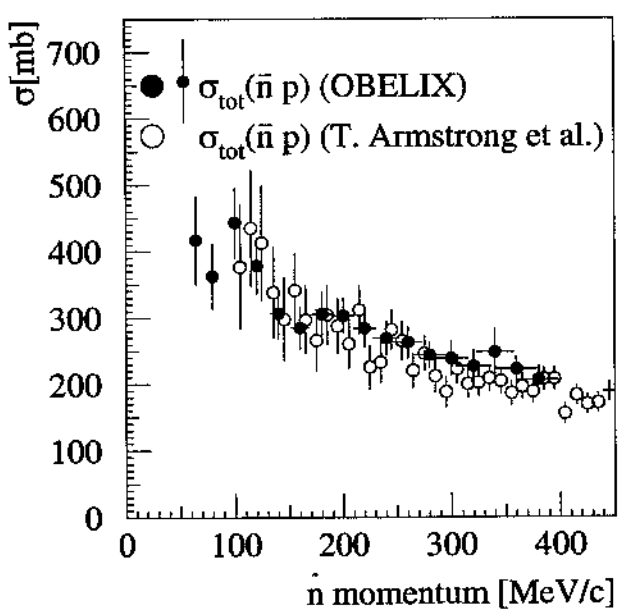

Figure 1.1: comparison of $\bar{n}p$ total cross section at low momenta: •: Ref. [1], ○: Ref. [2].

published data existing so far by Armstrong *et al.* [2], starting at 105 MeV/c. In the overlap region the two sets of data agree well, although the OBELIX data, affected by errors 40% smaller that those by Armstrong *et al.*, show a smoother behaviour. In the momentum region from 50 to 100 MeV/c there is moreover an

evidence for a dip around 80 MeV/c. We notice that the OBELIX experimental technique (attenuation of a quite narrow $\bar{n}$ beam along a thick [25 cm] LH_2 target) is quite free from systematic errors. In particular, thanks to the event-by-event reconstruction of the momentum of the interacting $\bar{n}$ in the wide-band $\bar{n}$ beam ($50 \div 405$ MeV/c), all the data in the above momentum range were collected simultaneously during several runs in several years. There is no reason why an unexpected systematic error due to a malfunctioning of the experimental device (beam, target, electronics) could affect only the two points at 64.5 and 80 MeV/c. On the contrary data collected with $\bar{p}$ in the same momentum range may often be affected by instrumental errors not completely under control (different $\bar{p}$ beam settings, different target thicknesses, . . .). The annihilation cross section $\sigma_{ann}(\bar{n}p)$,

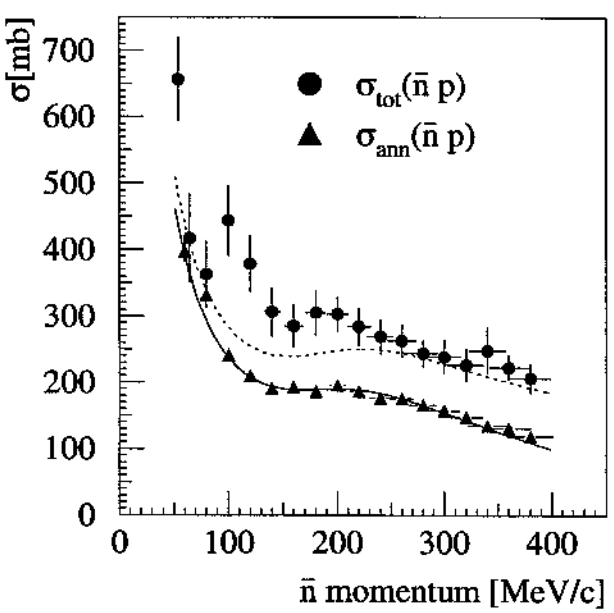

Figure 1.2: experimental values of the $\bar{n}p$ total (•) and annihilation (▲) cross sections. The curves represent evaluations of $\sigma_{ann}(\bar{n}p)$ and $\sigma_{tot}(\bar{n}p)$, as described in Ref. [1].

previously reported by OBELIX [3] shows on the contrary a smooth behaviour in the above momentum range, as shown in Fig. 1.2. These data were quite well reproduced by an Effective Range (ER) expansion calculation with the values of the parameters given by Mahalanabis *et al.* [4]. On the other hand the use of these parameters for describing the behaviour of $\sigma_{tot}(\bar{n}p)$ didn't give a satisfactory result at all ($\chi^2/ndf = 6.1$) as shown in Fig. 1.2.

In an analogous way, we could find several sets of parameters corresponding to different truncations of the ER expansion that fitted well $\sigma_{tot}(\bar{n}p)$, but failed

completely to reproduce $\sigma_{ann}(\bar{n}p)$.

The conclusion is that it seems impossible to find a set of parameters able to describe correctly at the same time both $\sigma_{ann}(\bar{n}p)$ and $\sigma_{tot}(\bar{n}p)$. The reason is that the elastic cross section $\sigma_{el}(\bar{n}p) = \sigma_{tot}(\bar{n}p) - \sigma_{ann}(\bar{n}p)$, shown in Fig. 1.3, exhibits an unexpected trend. A dip at low momentum is observed. The two points at 64.5 and 80 MeV/c are close to the lower bound imposed by the unitarity constraint for s-wave

$$\sigma_{el} \geq \frac{k^2}{4\pi}\sigma_{tot}^2 \tag{1.1}$$

where k is the c.m. $\bar{n}$ momentum.

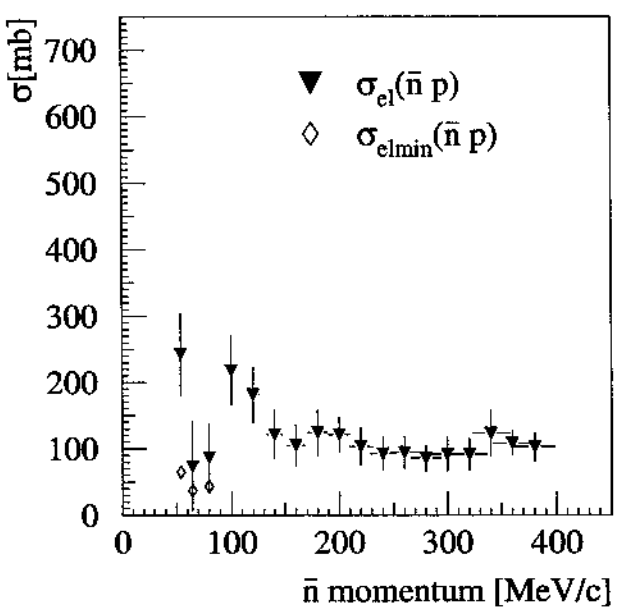

Figure 1.3: elastic $\bar{n}p$ cross section (▼) as a function of $p_{\bar{n}}$, obtained from the difference between total and annihilation cross section values; the diamonds represent the lower limits of the elastic cross section due to the unitarity constraints.

Another important conclusion inferred from the results of Ref. [1] is about the relative contributions of the I=1 and I=0 components of the $\overline{N}-N$ interaction. To this purpose the experimental value of $\sigma_{ann}(\bar{p}p)$ at 69.5 MeV/c are compared with the experimental values of $\sigma_{ann}(\bar{n}p)$ and $\sigma_{tot}(\bar{n}p)$ at the nearest momenta. The momentum value 69.5 MeV/c was chosen since a measurement of $\sigma_{ann}(\bar{p}p)$ exists [5] and this momentum is lower than the threshold of the charge-exchange channel ($p_{\bar{p}} = 98$ MeV/c) but quite high in order to minimize the effects due to the Coulomb interaction [6]. A straightforward observation is that the value of $\sigma_{ann}(\bar{p}p)$ (615 mbarn) is more than 50% higher than $\sigma_{tot}(\bar{n}p)$ ($\sim$ 400 mbarn) and 70% higher

than $\sigma_{ann}(\bar{n}p)$ ($\sim$ 350 mbarn). More quantitatively, the value of $\sigma_{tot}(\bar{p}p)$ obtained by the fit of Ref. [7] and of $\sigma_{tot}(\bar{n}p)$ obtained by the fit with ER approximation were compared. Even though not good for the physical interpretation, this fit may be considered just as a good numerical parameterization. At 70 MeV/c a value of 1.78 $\pm$ 0.25 was found for the ratio R $\equiv \sigma_{tot}(\bar{p}p)/\sigma_{tot}(\bar{n}p)$. By using the simple expression:

$$R \equiv \sigma_{tot}(\bar{p}p)/\sigma_{tot}(\bar{n}p) = \frac{\sigma_{tot}(I=0) + \sigma_{tot}(I=1)}{2\sigma_{tot}(I=1)} \tag{1.2}$$

in which $\sigma_{tot}(I=0)$ and $\sigma_{tot}(I=1)$ are the total cross sections related to the I=0 and I=1 components of the $\overline{\mathcal{N}} - \mathcal{N}$ interaction a strong dominance of the I=0 component at low momenta is observed. In fact the ratio $\sigma_{tot}(I=0)/\sigma_{tot}(I=1)$ is 2.5$\pm$0.4 at 70 MeV/c, to be compared to 1.1$\pm$0.1 at 300 MeV/c. This value is very close to the experimental ratio between $\sigma_{ann}(\bar{p}p)$ and $\sigma_{ann}(\bar{n}p)$ at 70 MeV/c, 1.76$\pm$0.11, which is simply the ratio between two experimental numbers, not resulting from extrapolations and parameterizations of data showing perhaps an unexpected behaviour.

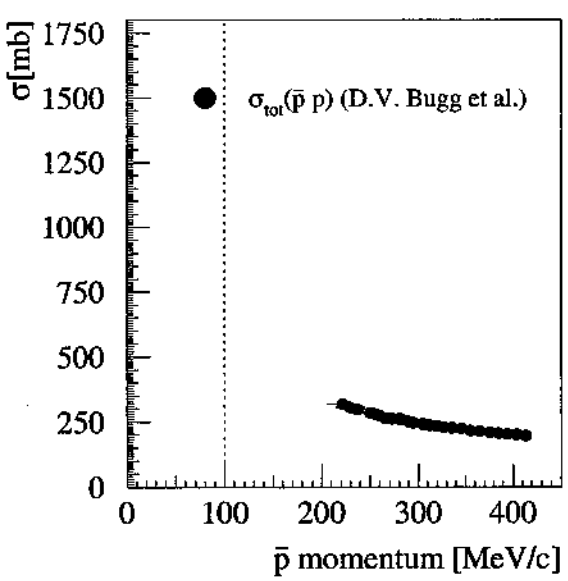

Figure 1.4: $\bar{p}p$ total cross section, from Ref. [7].

Following Dover *et al.* [8] this effect could be be a manifestation of the coherence of the ρ, ω, δ and σ meson exchange in the central tensor terms of the $\overline{\mathcal{N}} - \mathcal{N}$ medium range force. An indirect indication of such an effect following measurements in light nuclei was previously reported in [9].

ite surprisingly the data existing for the $\bar{p}p$ system are scarcer in the low mo-
Qu[illegible]n region. Total cross sections $\sigma_{tot}(\bar{p}p)$ are available down to 220 MeV/c [7]
g. 1.4), elastic cross sections $\sigma_{el}(\bar{p}p)$ were measured down to 181 MeV/c
(see Fi[illegible]nd there are good data sets for the annihilation cross section $\sigma_{ann}(\bar{p}p)$ be-
[10], a[illegible]0 MeV/c by OBELIX [11], [5] (see Fig. 1.5). Therefore there is no way to
low 10[illegible]ine $\sigma_{el}(\bar{p}p)$, even indirectly as for $\sigma_{el}(\bar{n}p)$.
determ

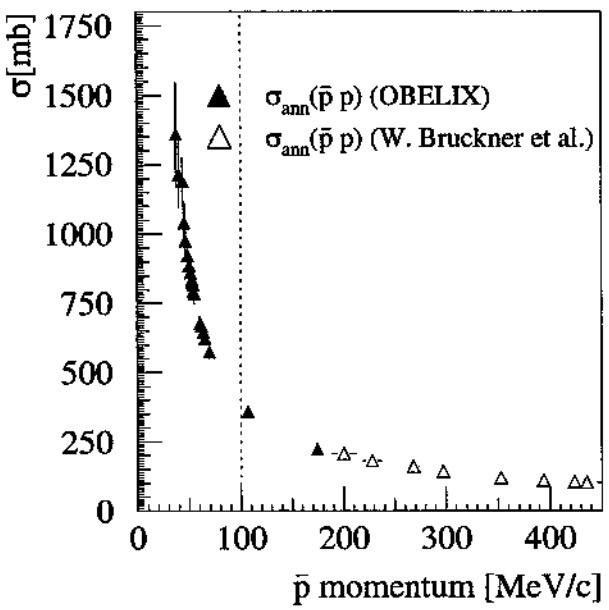

Figure 1.5: $\bar{p}p$ annihilation cross section, from Ref. [5](▲) and [10](△).

Taking into account that the elastic scattering amplitude for the $(\bar{n}p)$ system is pure isotriplet whereas for $(\bar{p}p)$ it is an equal-weight sum of the isosinglet and isotriplet amplitudes, we may expect to observe an anomalous behaviour also in $\sigma_{el}(\bar{p}p)$. Under the hypothesis that this anomalous behaviour is related only to the isotriplet amplitude, the effect on $\sigma_{el}(\bar{p}p)$ should be less spectacular, taking also into account the difference in the relative contributions of the two amplitudes at low momenta.

We remark that an unexpected behaviour of $\sigma_{el}(\bar{p}p)$ was already observed just at the edge of the momentum range covered by the above mentioned measurements of $\sigma_{el}(\bar{p}p)$, more precisely in the ratio ρ of the real to imaginary part of the forward scattering amplitude. The ρ-value was derived from the differential elastic cross sections by the Coulomb-nuclear interference method [12]. An oscillatory behaviour of the ρ-value was found below 300 MeV/c (see Fig. 1.6), not reproduced by dispersion relations [13] nor by recent optical model analyses [14].

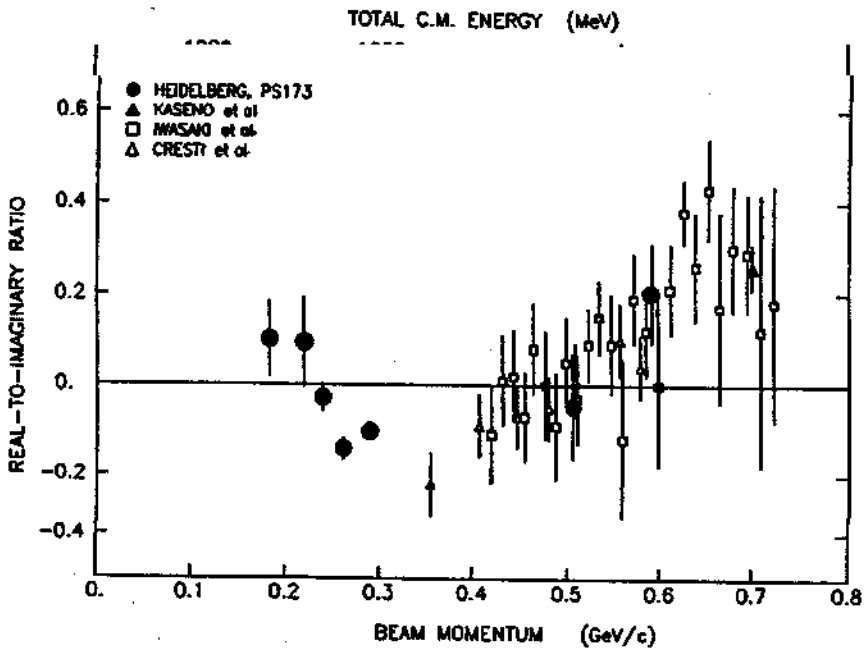

Figure 1.6: real–to–imaginary ratios of the $\overline{p}p$ elastic scattering amplitude, from Ref. [10].

A further experimental observation of a puzzling behaviour near the $\overline{\mathcal{N}}\mathcal{N}$ threshold was given by a dip in the $e^+e^- \rightarrow$ *hadrons* cross section as measured by FENICE [15] together with a steep rise in the proton time-like Form Factor (see Fig. 1.7). A good fit of both sets of data could be obtained [16] by introducing a narrow resonance interfering with the background given by broad resonances. The parameters of this state are $M = (1.87 \pm 0.01)$ GeV and $\Gamma = (10 \pm 5)$ MeV.

Further indications of structures around the $\overline{\mathcal{N}}\mathcal{N}$ threshold come from still unpublished $e^+e^- \rightarrow 6\pi$ data from the DM2 experiment and from the 6π diffractive photoproduction data from E831 at Fermilab [17].

Some years ago models have predicted $\overline{\mathcal{N}}\mathcal{N}$ bound states [18]. Several narrow resonances below threshold were predicted on the basis of a predominantly attractive $\overline{\mathcal{N}}\mathcal{N}$ potential, as deduced by means of the meson exchange model of the $\mathcal{N}\mathcal{N}$ potential and of the exchanged G parity. Recent overviews on this subject can be found in Refs. [19] and [20].

A very interesting and simple approach for an explanation of the above described anomalies was developed by Kudryavtsev and Druzjinin [21] in terms of scattering length s-wave approximation. They were able to explain qualitatively

the complete set of existing information at that time (only preliminary data from OBELIX on $\sigma_{tot}(\bar{n}p)$ were available [22], without the clear indication of the dip) and to predict the behaviour of the hadronic contribution to $\sigma_{el}(\bar{p}p)$ at low momenta, reported in Fig. 1.8. The main physical hypotheses in their calculation

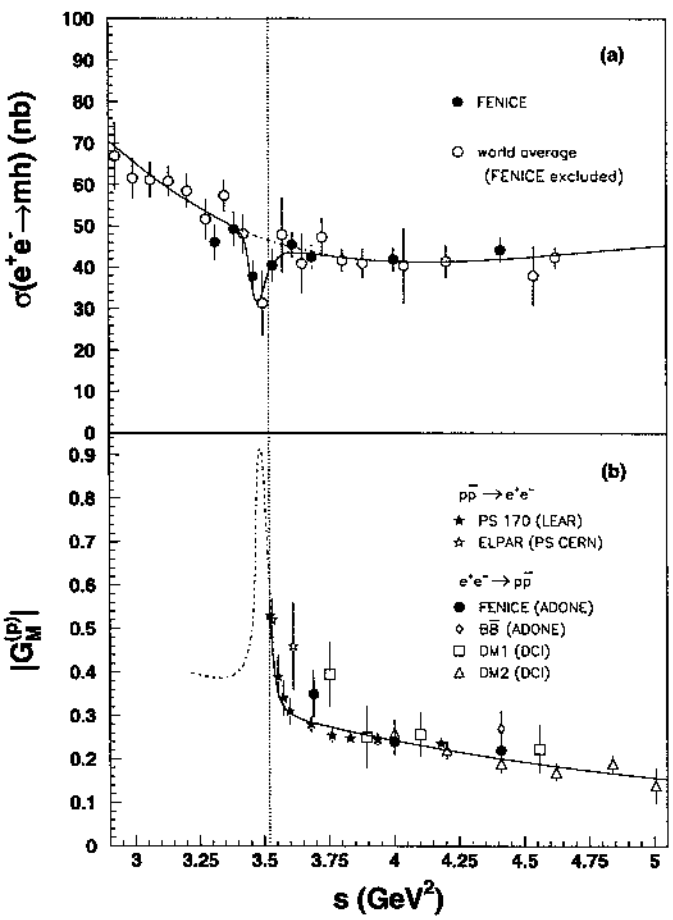

Figure 1.7: (a) Total $e^+ e^- \rightarrow$ *hadrons* cross section, systematics is also included in the error bars; (b) proton time-like Form Factor. The solid curves are the best fit assuming the interference with a resonance below the $\bar{N}N$ threshold (the dashed curve in (a) is the expectation without). From [16].

are:

i) the presence of the second $\bar{n}n$ channel (CEX reaction $\bar{p}p \rightarrow \bar{n}n$ in the $\bar{p}p$ system, with a $p_{\bar{p}}$ threshold at 98 MeV/c lab.). The importance of the CEX threshold was already mentioned in Ref. [10];

ii) a strong isospin violation between the I=0 and I=1 channels at low momenta (already confirmed by Ref. [1]), which introduces a relationship between the isosinglet A_0 and isotriplet A_1 scattering lengths. The conclusion is that A_0 and A_1 have relatively large values of the real parts, but with opposite signs. Consequently, the $\bar{p}p$ interaction at low momenta is repulsive, as furthermore mentioned in Ref. [14] but the $\bar{n}p$ interaction is attractive.

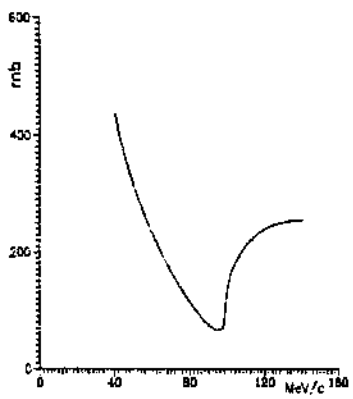

Figure 1.8: the $\bar{p}p$ elastic cross section, as predicted by [21].

These consideration led us to conceive a method to measure $(d\sigma/d\Omega)$ for $\bar{p}p$ hadronic elastic scattering at AD in the range 50-140 MeV/c.

Chapter 2

Principle of the method

The measurement of $\sigma_{el}(\bar{p}p)$ at AD from 50 to 140 MeV/c is not easy for at least two reasons:

i) the unambiguous identification of $\bar{p}p$ events needs a coincidence between the detection of an $\bar{p}$ (quite straightforward, due to the large energy deposit in any converter, with emission of several secondary particles: π, p) and of a very low energy proton [$(0 \div 3)$ MeV depending on the incident $\bar{p}$ momentum and the detection angle];

ii) the beam structure of AD (burst of $\bar{p}$, with a total number of $\bar{p}$ in the range $10^6 \div 10^7$, lasting at most 1 μsec, and with a repetition rate of some 10^{-2} Hz) prevents the use of beam counters and associated trigger logics. Furthermore, the detector must be *in vacuo* and a very thin solid target containing Hydrogen must be used.

Since we are interested to measure $\sigma_{el}(\bar{p}p)$ due to hadronic interaction, the forward cone dominated by Coulomb scattering will not be covered by the detector. At an incident $\bar{p}$ momentum of 50 MeV/c the laboratory angle for which the Coulomb and hadronic cross sections for elastic scattering are nearly equal is $\sim 35°$. At 25° lab. the Coulomb elastic scattering cross section is about 10 times larger than the hadronic one but such an effect is still tolerable to our experimental technique. At larger momenta the amount of the Coulomb scattering is greatly reduced. The angular range spanned by the detector will then be $25° \div 65°$ (lab.), $50° \div 130°$ in the center of mass. The upper limit is due to the fact that since the elastic process $\bar{p}p$ is symmetric with respect to the two particles, protons scattered by a lab. angle smaller than 25° would be lost.

We have conceived the following method in order to overcome the above limitations. Let us suppose that the $\bar{p}$ beam, of variable momentum (between 50 and 140 MeV/c) is well focused (beam spot ≤ 2 mm) onto the thin target. We suppose

furthermore that there is no beam halo at a distance of ~ 5 cm from the beam axis and then only particles interacting with the target reach the detector. The detector is shaped like a squared parallelepiped, ~ 10 cm wide and ~ 8.5 cm long, located with the front side at ~ 2 cm from the target. We may suppose that the particles' source following the $\bar{p}$ interaction is point-like. The detector is made by six adjacent layers of scintillating fibers, stretched parallel to the beam axis and orthogonal to it, following the stratigraphy shown in Fig. 2.1. For a simulation of the

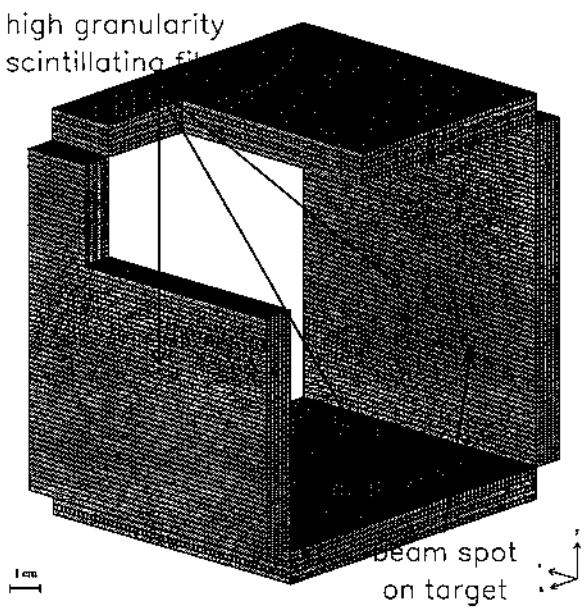

Figure 2.1: sketch of the scintillating fiber detector.

apparatus response, we have chosen squared fibers, of 1.5 mm side, but it is possible that further simulations and laboratory tests will lead us to change the shape and the dimensions of the elements. The fibers are viewed at one end by position sensitive photomultipliers (PSPM). The signals, suitably amplified, are read-out in parallel by a system of Flash Analog-to-Digital converters (FADC), which have a sampling time of 10 ns. The FADC clock is triggered by the machine at the beginning of the burst.

Then, during the burst length, up to 100 samplings of each channel of the fiber system may be obtained. If the total number of interactions in the target is of the order of $(30 \div 40)$/burst and the detector environment is not crowded by a huge number of undesired particles (annihilations of the $\bar{p}$ of the beam halo in the apparatus, pions from $\bar{p}$ annihilation along the beam line, upstream and downstream the target, and from the beam dump), events due to $\bar{p}p$ elastic scattering could be distinguished by topology from the annihilation events. The first topology looks

as shown in Fig. 2.2, *i.e.* an annihilation star originating from the first layer of fibers (the $\bar{p}$) with an isolated back-to-back hit (the p). The very short range of protons (a few tenths of microns) allows correlation only in one plane; to start we have chosen the (x-y) plane.

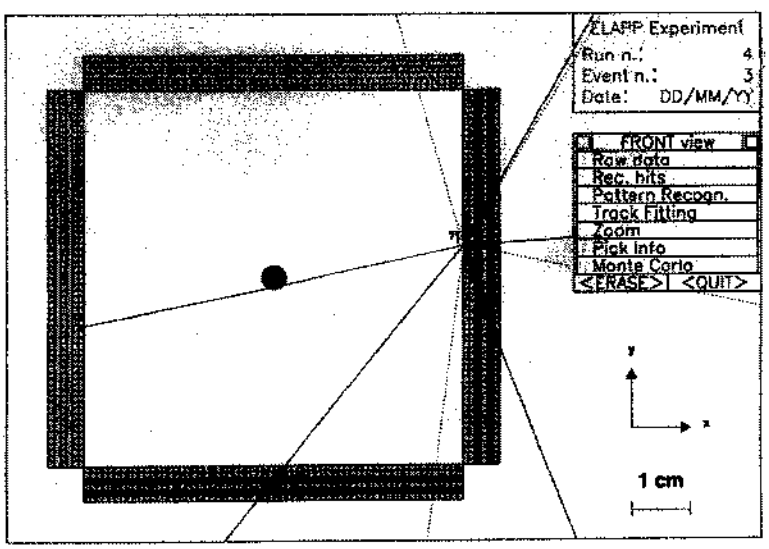

Figure 2.2: Monte Carlo simulation of the response of the detector for an $\bar{p}p$ elastic event.

The topology of an event corresponding to an $\bar{p}$ annihilating into the target (on a proton or ^{12}C) will be clearly distinguishable: at least two prongs originating from the target (see Fig. 2.3).

The interaction rate of events in the CH_2 target may be adjusted by a proper choice of the values of the target thickness and of the total number of $\bar{p}$ in the burst. Let us assume, as typical values for the cross section of $\bar{p}$ on p and ^{12}C in the range $50 \div 100$ MeV/c

$$\sigma_{tot}(\bar{p}p) \simeq 500\,\mathrm{mb}$$

and

$$\sigma_{tot}(\bar{p}\,^{12}C) \simeq 2600\,\mathrm{mb}\ (A^{2/3}\ \text{scaling law}).$$

The number of $\bar{p}$ interacting in the target N_{int} may be written as

$$N_{int} \simeq (N_{\bar{p}}\, x\, \rho) \times [\frac{2}{14} \times \sigma_{tot}(\bar{p}p) + \frac{1}{14} \times \sigma_{tot}(\bar{p}^{12}C)] \times N_A \qquad (2.1)$$

where $N_{\bar{p}}$ is the number of $\bar{p}$ per burst, x is the thickness of the target, ρ is the density of CH_2 (0.95 g/cm^3) and N_A is the Avogadro constant. If we express $N_{\bar{p}}$

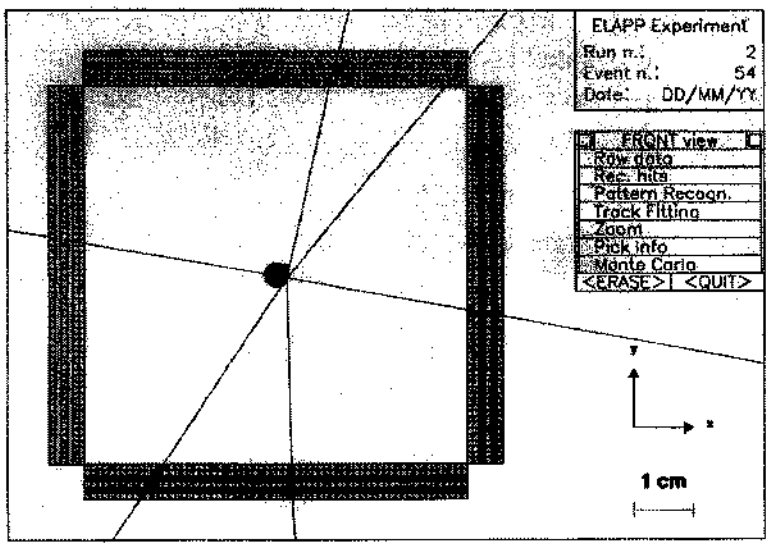

Figure 2.3: Monte Carlo simulation of the response of the detector for an $\bar{p}$ annihilation event.

in units of 10^6 and x in microns, we get:

$$N_{int} \simeq 16 \times (N_{\bar{p}}\, x\, \rho).$$

In an analogous way we may obtain the number N_{el} of elastic events seen by the detector by:

$$N_{el} = (N_{\bar{p}}\, x\, \rho) \times [\frac{2}{14} \times \sigma_{el}] \times N_A \times \Delta\Omega_1 \times \epsilon_1 \qquad (2.2)$$

If we assume $\sigma_{el} = 150$ mb, a solid angle $\Delta\Omega_1$ for elastic scattering 0.5 of the total solid angle and a reconstruction efficiency $\epsilon_1 \sim 0.5$ (see afterwards) we obtain:

$$N_{el} \sim 0.35 \times (N_{\bar{p}}\, \rho\, x)$$

then:

$$N_{el}/N_{int} \sim 2.2 \times 10^{-2}.$$

If we adjust $N_{\bar{p}}\, x$ in order to have ~ 40 interactions/burst, we will have ~ 0.9 $\bar{p}p$ elastic event per burst. We believe that this estimate is quite conservative: we assume that all events corresponding to N_{int} will be detected, ignoring annihilations in all neutral or with charged particles out from the geometrical acceptance of the detector.
The number of $\bar{p}p$ elastic events per day would be then $\sim 1.3 \times 10^3$, enough not only to determine the behaviour of $\sigma_{el}(\bar{p}p)$ as a function of $p_{\bar{p}}$, but also to ascertain whether it is pure s-wave scattering or a mixture of $s-$ and $p-$ waves.

Fig. 2.4 shows the trend of Montecarlo angular distributions for 2500 events (two days of data taking), for different hypotheses of s and p wave elastic scattering. The events have been generated in a $(50° \div 130°)$ acceptance angle in the center of mass, to appreciate the distortion brought by the p wave contribution. Fig. 2.4a) shows the angular distribution for the outcoming antiproton angle, evaluated in the center of mass, in the hypothesis of a pure s wave elastic scattering (isotropic distribution). Fig. 2.4 b), c), and d) show the same angular distribution in the three hypotheses $95 \div 5\%$ s/p, $90 \div 10\%$ s/p, and $85 \div 15\%$ s/p. The superimposed curves are fits of the distributions with a straight line (pure s

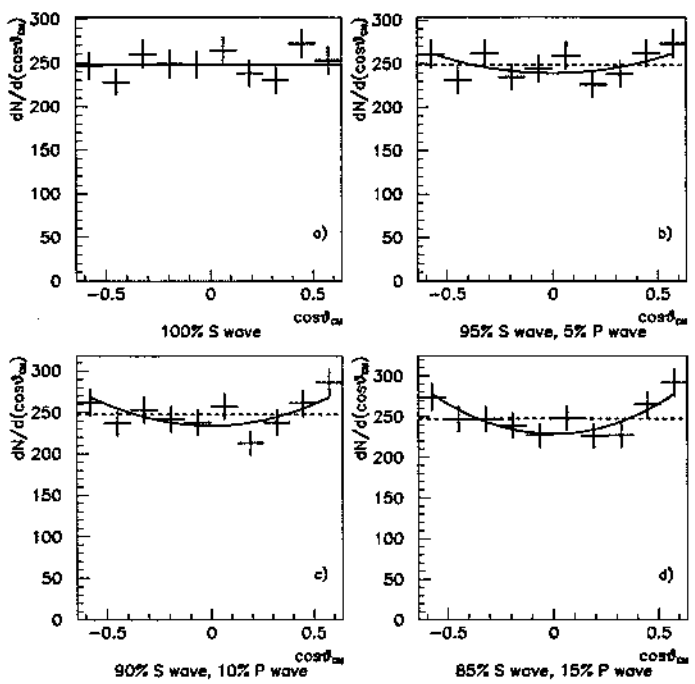

Figure 2.4: Distribution of the outcoming antiproton angle in the center of mass, for Montecarlo elastic scattering events generated in the detector acceptance in four different hypotheses of s and p wave population: a) 100% s wave, b) $95\% \div 5\%$ s/p, c) $90\% \div 10\%$ s/p, d) $85\% \div 15\%$ s/p. The superimposed curves are fits to the distribution with a straight line or with a parabolic function (see text).

wave hypothesis) or with a $a + b\cos^2\theta_{cm}$ function, corresponding to s and p wave admixture. Tab. 2.1 reports the confidence levels for the fits with a simple straight line in the b), c), d) cases. From this table, one can deduce that the distortion from

a flat distribution carried by p wave may be detected up to a limit of 5%, at 0.9 σ level.

s wave content	C.L. pure s wave fit
0.95	0.39
0.90	0.12
0.85	0.06

Table 2.1: Confidence Levels for angular distribution fits with a straight line (pure s wave hypothesis), for different of s wave contents in $\bar{p}p$ elastic scattering, in the detector acceptance.

Chapter 3

Experimental devices and techniques

3.1 Beam and experimental area

We need an $\bar{p}$ beam with variable momentum from $\sim$ 140 MeV/c down to $\sim$ 50 MeV/c. The beam must be reasonably "well momentum analysed" ($2 \div 4\%$), well focused ($\leq$ 2 mm), and with a small halo (no $\bar{p}$ from the beam at 5 cm from the axis at the focus [target]). Furthermore, the non-interacting $\bar{p}$ beam ($\geq$ 99.5%) must be transported to the beam dump, which has to be located at about 5 m from the detector in order to have a solid angle of at most 10^{-4} sr spanned on the main background pions source from the $\bar{p}$ annihilation. Some concrete blocks between the beam dump and the detector would be very desirable. The only accessible area for the experiment is the general purpose area (see Fig. 3.1), used for Machine Development with a dedicated beam line (DEM) and possibly by other experiments. We have then to try to find how, together with the AD machine staff, the main AD users (ATHENA, ASACUSA, ATRAP) and other possible small experiments, to cope with all these constraints. The ELAPP detector in itself is small, light, easy removable in a short time (less than half a day). The beam dump, containing also detectors for the absolute normalization, could be located in the small concrete cage indicated in the Figure, after a bending towards the AD ring wall.

For the incident $\bar{p}$ beam two different options (not alternative!) may be used. The momentum range from 100 MeV/c upwards can be covered with the existing DEM beam line, possibly with some changes concerning the focus on the target. We do not know how long is needed to the AD Staff for these settings (Fig. 3.1a)).

Antiprotons below 100 MeV/c may be obtained by degrading the primary beam by means of layers of suitable materials of variable thickness. A degrader produces inevitably a spread in momentum around the mean value (lower than the

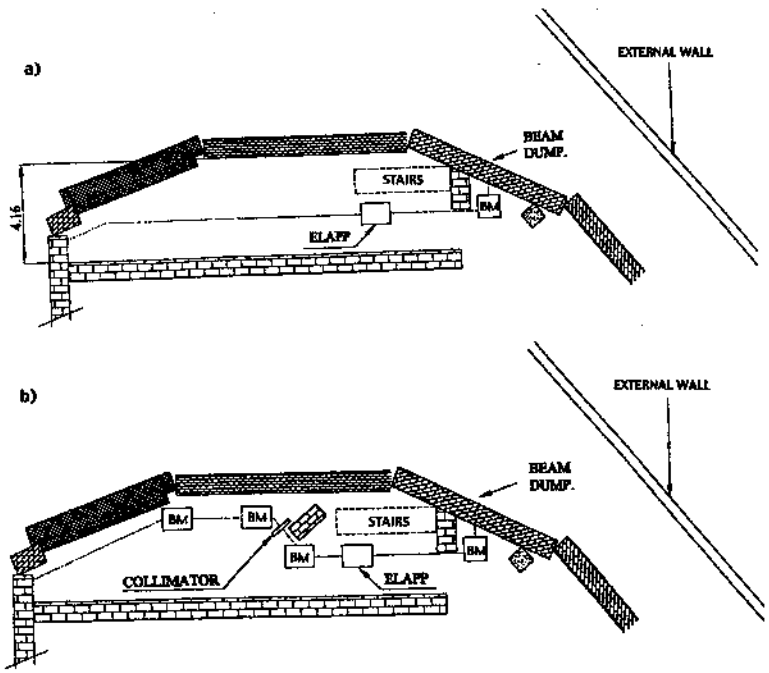

Figure 3.1: sketch of the DEM experimental area with a possible ELAPP location: a) direct beam (100÷140) MeV/c; b) degraded beam (50÷100) MeV/c. BM = bending magnet.

incident one) and an angular spread, both the quantities increasing with its thickness and an attenuation (quite negligible). Table 3.1 reports the thicknesses of a suitable material (Mylar) necessary to decrease the 100 MeV/c $\bar{p}$'s to the desired lower average momentum, the r.m.s. angular divergence, the r.m.s. momentum spread and the attenuation due to interaction.

After the degrader, an analyzing magnet must disperse the beam on a suitable slit, with variable opening, that could be the source for a following magnetic device able to focus the $\bar{p}$ onto the target.

We have not studied yet the best conditions for the construction of such a beam (bending angles, quadrupoles or solenoids as focusing devices, ...). We guess that the transmission of such a device to the target could be at best 20% ($N_{\bar{p}} \leq 2$). We also do not know which are the best conditions fulfilling the need of the DEM area (mobile beam elements, dedicated line close to the wall facing the AD machine, see Fig. 3.1b)).

The beam monitor will be located in the beam dump. Here we expect to have a large amount of particles (pions) $\sim 10^7$ in total with instantaneous rates of 10^{13} s^{-1}, that can be monitored:

$\bar{p}$ momentum (MeV/c)	degrader thickness (μm)	σ_θ (degree)	σ_p (MeV/c)	attenuation
95	51	0.85	0.38	$0.75 \cdot 10^{-3}$
90	96	1.32	0.52	$1.4 \cdot 10^{-3}$
85	136	1.79	0.66	$2.0 \cdot 10^{-3}$
80	170	2.28	0.78	$2.6 \cdot 10^{-3}$
75	199	2.83	0.90	$3.1 \cdot 10^{-3}$
70	223	3.45	1.02	$3.5 \cdot 10^{-3}$
65	243	4.18	1.16	$3.9 \cdot 10^{-3}$
60	259	5.04	1.29	$4.2 \cdot 10^{-3}$
55	273	6.08	1.43	$4.5 \cdot 10^{-3}$
50	283	7.47	1.61	$4.7 \cdot 10^{-3}$
45	292	9.10	1.79	$5.0 \cdot 10^{-3}$

Table 3.1: thickness of Mylar necessary to decrease 100 MeV/c $\bar{p}$'s to the indicated lower average momentum; the r.m.s. multiple scattering deflection (σ_θ), the r.m.s. degrader straggling (σ_p) and the attenuation of the primary beam are also reported.

i) by detecting the integrated light output with a suitable device: scintillating fibers or scintillators and HPD or CCDs;

ii) by single counting with a small area device subtending a very small $\Delta\Omega$ ($< 10^{-5}$ sr): scintillating fibers/PSPMs.

Probably a combination of the two devices will be the best compromise, with the aim of knowing the relative burst intensity to $\sim 2\%$, the absolute one to $\sim 10\%$. An overlap point between the two beam settings will be necessary. For instance $\sigma_{el}(\bar{p}p)$ at 100 MeV/c could be measured both with the primary beam setting and with the degraded beam setting (direct beam at 130 MeV/c and a suitable degrader).

3.2 Targets

As previously mentioned we need to use a solid target containing H_2, and a dummy target containing the same amount of atoms/cm^2, excluding H. The obvious, well known solution is CH_2 (polyethylene) and C for the dummy target. In our case the thicknesses are ~ 10 μm of CH_2 and ~ 5 μm of C. These thin targets have to be supported and stretched by some mechanical frame, which must be as large as possible in order to avoid the (few) beam halo $\bar{p}$'s interact on it. The best solution would be a square frame whose side is as long as the fibers' box one.

It is possible to stretch CH_2 and C foils of the above mentioned thicknesses even without additional strengthening wires, according to the experience of other Laboratories. Some care will be necessary for the transportation of the C targets, in vacuum-sealed containers.

A different problem will be the determination of the thickness and homogeneity of both thin targets, at least in the $\sim$ 1 cm^2 area irradiated by the beam, in order to be able to perform a correct subtraction. We will investigate how to fulfill these requirements.

Another way to obtain solid targets containing Hydrogen is to use films of $Si_{1-x}C_xH$ with techniques developed at the Politecnico di Torino [23]. The advantage is that in this case the dummy target $Si_{1-x}C_x$ is obtained from the same sample used for $Si_{1-x}C_xH$ by chemical methods and the thickness for the subtraction technique is guaranteed to 2%. Moreover, the atomic structure of the samples will be tested by α particles backscattering. Furthermore there are apparently no particular problems in getting the above films already supported by a Si frame. The main disadvantage in using these targets is that the H/$Si_{1-x}C_x$ ratio is 1 instead of 2 as for CH_2, and moreover Si has a larger annihilation cross section as compared to C. We consider then such a choice as a back-up solution in case of insolvable problems in the C foils handling.

3.3 Scintillating fiber assembly

The detector must fulfill several severe constraints:

i) a detection threshold of energy deposited by stopping protons as low as possible (0.5 MeV). This feature affects strongly the capability of the detector to cover the full angular range even at the lowest incident $\bar{p}$ momentum ($p_{\bar{p}}$ = 50 MeV/c $\leftrightarrow$ $Tp_{\bar{p}}$ = 1.33 MeV). Fig. 3.2 shows the limits of detection imposed by the threshold on the energy deposited by the proton (0.5 MeV) in measuring the differential cross sections. We have studied the response of thin scintillators, 0.15 x 0.15 x 10 cm^3, irradiated with low energy protons (0.4 - 2.0 MeV). The main purpose was that of checking experimentally the non linearity of the response to highly ionizing heavy particles. The measurements were performed in two subsequent short runs at the Van der Graaf machines of Legnaro and Firenze. At Legnaro the detector was in air and very low energy protons (up to 0.4 MeV) were obtained by degrading with suitable thicknesses of materials a continuous proton beam of variable energy, but always higher than 1.9 MeV. The above energies are affected by an incertitude of 0.1 MeV due to straggling. At Firenze the detector was in vacuo and the energy of proton known to 0.01 %, but the beam, optimized

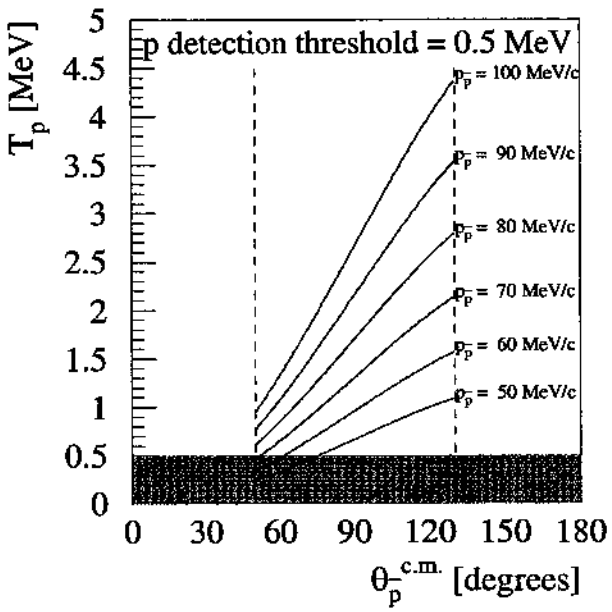

Figure 3.2: angular range (in the C.M. system) covered by the ELAPP detector. The continuous lines show the capability of detecting a p in the selected angular region (vertical lines) versus the momentum of the incident $\bar{p}$, in the hypothesis of a detection threshold of 0.5 MeV (shadowed area).

for other applications, had a quite complicated time structure (bursts of 1 ns with a "statistically" predetermined number of protons in the burst). By combining the results of the two runs, the final result shown by Fig. 3.3 was obtained. It appears that we may assume a detection limit for protons of 0.5 MeV as a quite conservative figure.

ii) high granularity. The first layer is the most critical one: it has to detect both the stopping proton (isolated hit) and the stopping $\bar{p}$ (starting point for the pattern recognition algorithm), with high efficiency and low threshold. It is hard to think for such a layer to elements different from square shaped scintillators, 1.5 mm wide, $\sim$ 8.4 cm long. A surface cold deposition of Al on the three sides not facing the inner region would be helpful in order to increase the light collection. The following layers can be of square or circular shape; their main prerequisite is the granularity for an efficient tracking of pions from $\bar{p}$ annihilations, with a reduced number of planes. The light emitted from each scintillating element is transported through white optical fibers, having the same cross section and a length of $\sim$ 25 cm to the cathode of a PSPM Hamamatsu type H7546 with 64 pixels. The connection between

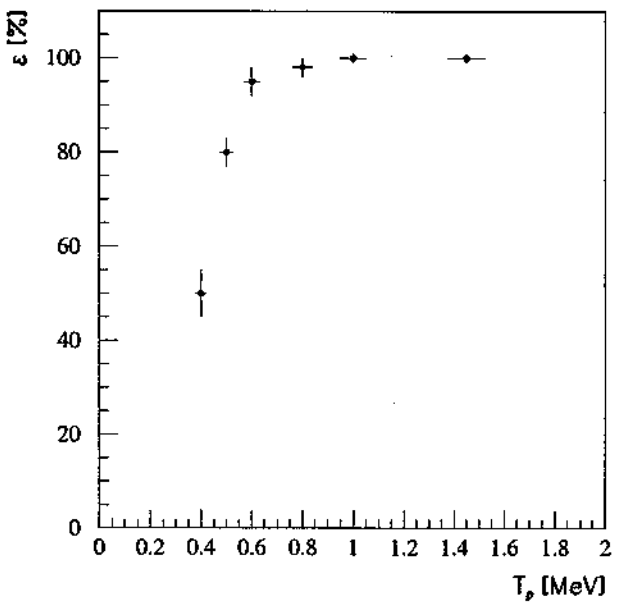

Figure 3.3: detection efficiency of prototype scintillators as a function of the incoming proton kinetic energy obtained from the tests in Legnaro and Firenze.

the scintillating fiber and the white one may be obtained by glueing or with optical contact (estimated loss $\leq 20\%$).

Studies are required for glueing, mechanical supports and other mechanical items necessary in order to strengthen the full structure. Care also has to be devoted to the optical contact between the fiber bunches and the PSPM, having in mind that the scintillating fiber assembly is in vacuo.

3.4 Front-End Electronics

The present typical gain of Hamamatsu H7546 with 64 pixels is 10^6, the cross-talk between adjacent pixels is $\sim 3 \div 5$ %, and the non-homogeneity of response among various pixels is less than a factor 3. The photocathode efficiency is at present $\sim$ 20 %. These performances fulfill the needs of the experiment. The front-end electronics (FEE) of each channel is composed by an amplifier with bandwidth of 100 MHz and a FADC with 8 bit resolution, with 100 MHz sampling rate, with non-linear response extending the dynamic range to 10 bits. It is necessary to introduce a voltage amplifier (or a current amplifier with variable gain) with output compensated for the attenuation due to the length of the twisted pair cable, between the output of the PSPM and the digitizing system. Taking an

average number of 10 photoelectrons (with a cathode efficiency of 20%) [24] a gain of the PSPM of 10^6 and a pulse width of 10 ns, we get a pulse height of 8 mV on 50 Ω, corresponding to a charge of 1.6 pC. The FADCs accept signals up to 1 V and then the signals from the PSPM have to be amplified by a factor $10 \div 50$ in order to exploit the full dynamic range. This requires the design of an integrated low noise amplifier with a bandwidth of 100 MHz. Two prototypes of the fast amplifiers have been already designed. Fig. 3.4 shows a scheme of one of these, already built and under test. They will be housed in customized 6U VME boards. Each board may accomodate up to 24 amplifiers and a crate may accomodate 20 boards, for a total of 480 amplifiers. All the amplifiers needed for the experiment could be housed in a rack in between the two racks housing the FADCs.

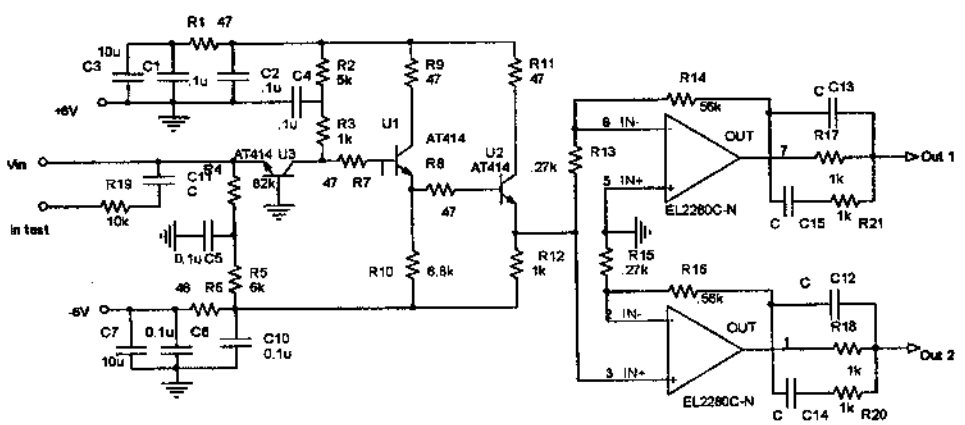

Figure 3.4: scheme of the current amplifier designed for the ELAPP experiment.

We describe now briefly the digitizing system with FADCs [25]. Each channel (fiber) is continuously digitized by a FADC, with sampling time of 10 ns, and the result of the conversion is stored in a circular memory of 256 bytes, i.e. for a time of 2.56 μs.

A customized crate (DL350) contains:

i) 176 FADC channels, housed in 22 modules;

ii) a programmable clock fan-out and address generator module (SAM) which drives in parallel the circular memory and the FADC during the sampling phase;

iii) a zero-suppressor module, which reads sequentially the circular memories (SIM) after the sampling phase;

iv) a module containing two digital signal processors (DSP) able to perform analyses of the data read out from the circular memories.

A STOP signal at the end of the $\bar{p}$ burst stops the conversion of the FADCs and triggers the read-out of all the hits recorded by the detector. This operation starts with the zero-suppression by means of the SIM, which reads the circular memories, compares them with a programmed threshold and stores them in a multilevel-buffer. After the read-out the system returns to the active status. The read-out time depends on both the number of FADC in the crate and the number of hits recorded by the detector and it may be evaluated in less than 5 ms. In the same time the data collected in the buffer may be sent to the DSP for linearization, base-line calculation, noise evaluation, time and charge evaluation.

For ELAPP, at least in the debugging phase, these algorithms may not be implemented in the DSP thanks to the long time between the bursts (up to 60 s). This circumstance allows the direct transmission of all the collected hits directly to the central CPU.

The FADC system can be divided into two groups of 5 DL350 crates, connected through a STR723 board to a local VSB bus and then to a CES FIC8234 CPU, running the Local Event Builder (LEB). The data read by LEBs will be sent through VME bus to the Global Event Builder (GEB), which resides in a LynxOS CPU. The two LEBs and the GEB will be housed in the same VME crate. The Run Control process will run on a Linux PC and will communicate with the other processes via socket based network protocols. Data will be written both on disk for monitoring purposes and on tape. Some events will be sampled by GEB and sent to the monitoring processes through UDP sockets. The Online Monitor, useful to check continuously the detector performances, will be based on an object oriented approach in the framework of the ROOT package.

Finally we put forward a few remarks on the calibration of the apparatus. The FADC system is driven by a unique 100 MHz clock, but due to the differences in the propagation time along the bus and also to the small differences among the various channels, it is necessary to calibrate individually each channel both in time and in charge.

The amplifier, coupling the PSPM and the FADC, will provide a test signal for this calibration. The response of the 24 PSMSs must be measured and stored in a data base and the homogeneity in the transmission of the optical part must be checked periodically with the response to m.i.p. (cosmic rays). The time (60 s) between two bursts could be used to acquire events due to cosmic rays crossing the detector, triggered by a suitable scintillator hodoscope.

In conclusion we may expect the following: the efficiency per hit of each plane of fibers for m.i.p. is expected to be larger than 90 % [26]. The availability of PSPMs with a higher photocathode efficiency could improve the performance

and the reliability of the whole system.

The proposed system is in large part available (from Obelix experiment); however it can be built with commercial components.

3.5 Ideas for the Pattern Recognition

We approached the study of the pattern recognition by using a simple event generator, which takes into account the π multiplicities corresponding to $\bar{p}p$ annihilations. With the implemented generator, we have evaluated roughly the pattern recognition efficiency for the $\bar{p}p$ elastic events (an $\bar{p}$ annihilation star with an back-to-back isolated hit) and we found $\epsilon_1 \approx 50\%$. On the other hand the efficiency for detecting an $\bar{p}$ annihilation in the target (at least two prongs originating from the target) was found to be $\epsilon_2 \approx 18\%$. These evaluations were done by a visual scanning. The developing and the coding of the pattern recognition algorithms is in progress. They are based on "increased density" patterns in the detector: first a fiber of the first layer which delivered a "high" light output, due to the stopped $\bar{p}$ and to the annihilation prongs is looked for; then a back-to-back isolated hit in the first layer must be found, corresponding to the stopped p; finally starting from the fiber where the $\bar{p}$ annihilated, the annihilation prongs will be tracked.

A further step in the pattern recognition development will be the test of its robustness against the presence of background signals. Indeed π hits belonging to $\bar{p}$ annihilated "somewhere" (collimator, beam dump, beam pipe, ...) could overlap a "genuine" elastic event. A possible improvement could be the use of neural networks to filter the events.

3.6 Normalization of the cross section

The main physics interest of the measurement is the search for a dip-bump structure in $\sigma_{el}(\bar{p}p)$, compared to a smooth behaviour of $\sigma_{ann}(\bar{p}p)$ and $\sigma_{ann}(\bar{p}\,^{12}C)$. Events due to $\bar{p}\,^{12}C$ elastic scattering will not be considered since their topology is the same of an $\bar{p}$ in the beam halo interacting in the detector. About 18% of the $\bar{p}$'s annihilating in the target ($\sim$ 80% of the total number of interacting $\bar{p}$'s) will give at least two prongs seen by the detector (see Fig. 2.3) and could be used for the determination of $[\sigma_{ann}(\bar{p}p) + \sigma_{ann}(\bar{p}\,^{12}C)]$. Then we will have at least 10^4 annihilation events/day, in the above conditions.

In order to disentangle the contributions of $\sigma_{ann}(\bar{p}p)$ and $\sigma_{ann}(\bar{p}\,^{12}C)$ it is necessary to perform an ancillary measurement with a thin ^{12}C foil, of thickness equivalent to that one of the ^{12}C nuclei in the CH_2 target, lasting $\sim$ 1/2 day. This way we will have the following quantities, normalized to the total $\bar{p}$ flux, measured

with the beam monitor near the beam dump

$$\sigma_{el}(\bar{p}p)\Delta\Omega_1\epsilon_1,$$

$$\sigma_{ann}(\bar{p}p)\Delta\Omega_2\epsilon_2,$$

$$\sigma_{ann}(\bar{p}^{12}C)\Delta\Omega_2'\epsilon_2',$$

in which $\Delta\Omega$ is the solid angle for the detection of the corresponding reaction (note $\Delta\Omega_1 \sim 3\,\Delta\Omega_2$) and ϵ the detection efficiency, including the pattern recognition efficiency. $\Delta\Omega_2 \approx \Delta\Omega_2'$, $\epsilon_2 \approx \epsilon_2'$. $\Delta\Omega$ and ϵ will be determined by suitable MC simulation. Then, by using the known values of $\sigma_{ann}(\bar{p}p)$ [11] [5] it will be possible to obtain absolute values for $\sigma_{ann}(\bar{p}^{12}C)$ and, mainly, $\sigma_{el}(\bar{p}p)$, with an error not exceeding 5 %.

Chapter 4

Possible extensions of the Physics Program

The motivating physics program for the experiment is the measurement of $\sigma_{el}(\bar{p}p)$ in the $50 \div 140$ MeV/c range. A by-product will be the measurement of $\sigma_{ann}(\bar{p}^{12}C)$ in the above momentum range.

A similar set of data (σ_{el} and σ_{ann}) could be obtained for the Deuterium by using a CD_2 target, that can be produced at the desired thicknesses. The measuring time could be reduced since there is no need to perform a measurement with a dummy ^{12}C target (being already performed for the CH_2 data).

Finally a survey of σ_{ann} on nuclear targets (solids that can be machined in thin foils) may be obtained in a short time (3% statistical error per target and per momentum setting in 5 hours).

Chapter 5

Planning of the experiment and beam requirements

In the following we outline shortly a possible scenario that optimizes the needs of the experiment. Clearly it has to be adapted to the needs of AD and of the already approved experiment. The more crucial point, to our opinion, is the setting-up of two beam lines: one for (50÷100) MeV/*c* the other for (100÷140) MeV/*c*.

- 2001:
    1. Test of the halo in the (100÷140) MeV/*c* beam line with a short run (few hours) at 100 MeV/*c* at the existing DEM line with a simple device (scintillators at 5 cm from the focus, in vacuo).
    2. Completion of the mechanical design of the detector.
    3. Completion of the study on the feasibility of the beam line with the degrader (50÷100) MeV/*c*.
    4. Completion of the studies on fiber glueing, optical contacts, ..
    5. If (4) is successful, start-up of the assembly of the detector.
- 2002:
    1. Completion of the detector
    2. Calibration with protons at Legnaro and/or Firenze
    3. Installation at AD
    4. Measurements in the 100÷140 Mev/c range (60 hours for each momentum setting, 300 hours in total)
- 2003:

1. Analysis of the data
2. Setting-up of the beam line with the degrader (50÷100 MeV/c)
3. Measurements in the 50÷100 MeV/c range (60 hours for each momentum setting + 1 check point between the two beam lines - 100 MeV/c obtained by degrading a 130 MeV/c primary beam). 400 hours in total.

We are prepared to perform the above measurements whenever suited to the AD scheduling (nights, week-ends ..) and how required (self-users, ad-hoc operators, ...).

The installation is very easily removable (1/2 day) concerning the detector. A study has to be done for the degraded beam, in 2003.

For the counting barrack we need a 20 m^2 area.

Chapter 6

Final remarks

We are fully aware of the special agreements under which AD is running for the approved experiments and we are ready to negotiate with CERN and with INFN how to fulfill the necessary requirements, if the experiment is approved. We have already presented at the Nuclear Physics Committee (Commissione III) of INFN our letter of intent and a draft of the proposal and we obtained partial financial support for the presentation of the proposal and for part of the needs for 2001. We know that other Groups are willing to join the proposal, if approved.

Bibliography

[1] OBELIX Collaboration, F. Iazzi *et al.*, *Phys. Lett.* **B475** (2000) 378.

[2] T. Armstrong it et al. it Phys. Rev. **D36** (1987), 659.

[3] OBELIX Collaboration, A. Bertin *et al. Nucl. Phys. (Proc. Suppl.)* **B 56A** (1997) 227.

[4] J. Mahalanabis *et al.*, *Nucl. Phys.* **A485** (1988), 546.

[5] A. Zenoni *et al.*, *Phys. Lett.* **B461** (1999) 405.

[6] J. Carbonell *et al.*, *Phys. Lett.* **B369** (1996) 77.

[7] D.V. Bugg *et al.*, *Phys. Lett.* **B194** (1987) 563.

[8] C. B. Dover, T. Gutsche, M. Maruyama, A. Faessler *Prog. Part. Nucl. Phys.* **29** (1992) 87.

[9] F. Balestra *et al.*, *Nucl. Phys.* **A481** (1989), 572.

[10] W. Brückner *et al.*, *Phys. Lett.* **B166** (1986) 113.

[11] OBELIX Collaboration, A. Bertin *et al.*, *Phys. Lett.* **B369** (1996), 77.

[12] W. Brückner *et al.*, *Phys. Lett.* **B158** (1985) 180.

[13] H. Iwasaki *et al.*, *Nucl. Phys.* **A433** (1985), 580.

[14] A. Bianconi *et al.*, **Phys. Lett. B483** (2000), 353.

[15] A. Antonelli *et al.*, **Phys. Lett. B365** (1996), 427.

[16] A. Antonelli *et al.*, **Nucl. Phys. B517** (1998), 3.

[17] R. Baldini, private communication

[18] L.N. Bogdanova, O.D. Dalkarov and I.S. Shapiro, *Ann. Phys.* **84** (1974), 261; G.C. Rossi and G. Veneziano, *Phys. Rep.* **65** (1980), 153.

[19] J.M. Richard, in *Proc. Workshop on Hadron Spectroscopy* (Ed. T. Bressani, A. Feliciello, A. Filippi), Frascati Physics Series Vol. XV (1999), p. 413.

[20] F. Iazzi, in *Proc. Workshop on Hadron Spectroscopy* (Ed. T. Bressani, A. Feliciello, A. Filippi), Frascati Physics Series Vol. XV (1999), p. 659.

[21] A.E. Kudryavtsev and B. L. Druzjinin, ITEP–23–94.

[22] A. Adamo *et al.*, **Nucl. Phys. A558** (1993), 137.

[23] F. Demichelis *et al.*, *Physica* **B225** (1996), 103; P. Rava *et al.*, J. Appl. Phys **80** (1996), 4116.

[24] H. Leutz, *Nucl. Instr. Meth.* **A364** (1995) 422,
C. D'Ambrosio *et al.*, CERN-PPE/96-65.

[25] F. Balestra *et al.*, *Nucl. Instr. Meth.* **A323** (1992) 523.

[26] F. Balestra *et al.*, *Nucl. Instr. Meth.* **A426** (1999) 385.